Hindawi
Advances in Materials Science and Engineering
Volume 2019, Article ID 4561631, 16 pages
https://doi.org/10.1155/2019/4561631

Research Article

Study on the Seismic Performance of Box-Plate Steel Structure Modular Unit

Hui Mao,[1] **Guang-chong Qin**,[2] **and Tao Lan**[2]

[1]*School of Civil Engineering, Qingdao University of Technology, Qingdao 266033, Shandong, China*
[2]*China Shipbuilding Industry Corporation International Engineering Co., Ltd., Beijing 100021, China*

Correspondence should be addressed to Tao Lan; qd_lantao@163.com

Received 7 December 2018; Revised 14 March 2019; Accepted 10 April 2019; Published 2 May 2019

Academic Editor: Dora Foti

To study the seismic performance of the box-plate steel structure system, two three-storey single box-plate steel structure space stress-bearing unit test pieces have been designed and fabricated according to the 1 : 3 reduced scale. In addition, the quasi-static loading test has been performed on the test pieces where the destruction process, destroy mode, bearing capacity, hysteretic behavior, etc., have been studied and the impact of reinforcing measures with a corner or not on the seismic performance of test pieces has been mainly analyzed. The test results show that the destruction of the box-plate steel structure modular unit under the low cyclic loading effect starts with corner buckling and ends with corner wallboard tear. The test piece has excellent bearing capacity and energy dissipation; the corner reinforcing structure measure also has enhanced the seismic performance of the modular unit. Based on the test, we have taken finite element numerical simulation to the test pieces, compared the analysis result of the test with the finite element, and verified the effectiveness of the finite element analysis method. This paper designs four groups of 64 finite element model test pieces and discusses the influence law of the height-thickness ratio of the wallboard, flexibility coefficient of corner reinforcing structure rib, and axial compression ratio to the seismic performance of the modular unit. The results show that the bearing capacity of the test piece is decreased with the increase of axial compression ratio under the premise that the wallboard height-thickness ratio and flexibility coefficient of the corner reinforcing structure rib are certain. Based on the above analysis results, we have put forward the lateral force resistance calculation model of the reinforcing structure modular unit with or without corner.

1. Introduction

Steel plate shear wall, as a new type lateral force resistance structure system, has large lateral resistance stiffness and good seismic performance, which has been widely applied in the high-rise structure system [1–4]. The typical steel plate shear wall is composed of an embedded steel plate and surrounding steel frame. The embedded steel plate and frame are connected by a splice bar as transition and then connected through welding or high-strength bolt. The steel plate only bears the horizontal load, and the steel frame assumes the vertical load is borne by a steel frame [5–8].

In recent years, relevant scholars have taken great number of studies regarding the steel plate shear wall. Elgaaly [9] studied the seismic performance of stiffener-free thin-walled steel plate shear wall, and the result showed that the inelastic behavior of the thin plate test piece is mainly controlled by the thin plate yield strength, and the nonlinear characteristic is mainly related with the plate's tensile strength and diagonal tension field. Driver et al. [10, 11] studied the bearing capacity of the four-storey single steel plate shear wall test piece under strong earthquake, and the result indicated that the shear wall showed excellent ductility and energy dissipation characteristic. Kosari et al. [12] also studied the seismic performance of the high steel plate shear wall system. He stressed the high-order modal pushover analysis and discussed the corresponding pushover curve.

In addition to the typical steel plate shear wall, relevant scholars also have studied a great number of improved steel plate shear walls. All the steel plate concrete composite shear

wall and double-steel plate concrete composite shear wall studied by Nguyen and Whittaker [13] and Elmatzoglou and Avdelas [14] present excellent seismic performance. Borello [15] studied the joint steel plate shear wall (SPSW-WC) system, which also exhibited good seismic performance. Dastfan and Driver [16] studied the large steel plate shear wall with partly wrapped composite material (PEC) column and reduced beam (RBS) frame and put forward the RBS connection mode, which not only has reduced the requirement of beam column connection but also enhanced the seismic performance. Wang et al. [17] and Wei et al. [18] studied the lateral resistance performance of the corrugated steel shear wall under the horizontal force effect. The test results showed that the corrugated steel plate shear wall has the advantages of high bearing capacity, strong antishear buckling ability, sufficient hysteresis loop, and stable energy dissipation. Ozcelik and Clayton [19] studied a kind of steel plate shear wall with beam connecting web (B-SPSWs). As a kind of an improved structure system of steel plate shear wall (SPSWs), the web of which is only connected with the beam. The web and column have been separated in the B-SPSW, and simple beam column connection has been introduced, which has eliminated the web tension field's bending effect to column. The research results showed that B-SPSW has outstanding antibending performance under the seismic effect.

The box-plate steel structure system [20] studied in this text is a new type steel plate wall structure. The box-plate steel structure system is composed of a modular unit enclosed by the stiffened wall and the stiffened floor, which bears both the vertical and horizontal loads of the building, where the stiffened wall and the stiffened floor are all composed of steel plate, T-stiffener, and L-stiffener. There are no obvious beams and columns in the box-plate structure compared with the traditional steel plate wall. Few studies have been done on the box-plate structure system in the construction industry. The design of this structural system is based on the superstructure of ships [21]. The superstructure of ships will bear wind load and other effects, while the building structure on land needs to consider the seismic effect in the seismic fortification area. In this paper, a typical spatial stress element is selected to study its seismic performance, and the corresponding bearing capacity calculation formula and structural measures are proposed. At present, we combine the structural system with the integrated architectural design of fire protection, sound insulation, and heat insulation and apply the research results to the residential construction, as shown in Figure 1.

The structural system is described as follows: its wallboard is a steel plate in which one side is welded with vertical "L-" and "T-" shaped stiffener; the floor plate is a steel plate in which one side is welded with perpendicular "L-" and "T-" shaped stiffeners. The construction method of this structure has the characteristic of manufacturing in the factory and installation on the field. Under the background of vigorously developing building industrialization, the box-plate steel structure system, with the characteristics of easy for factory prefabrication, convenient for transportation, efficient in construction, high in quality, green, and environmentally friendly, is of great value. Different from the traditional steel plate wall structure, the steel plate wall with vertical ribs in the box-plate steel structure system needs to bear both the horizontal load and vertical load. To study the seismic performance of the box-plate steel structure system, two three-storey single box-plate steel structure unit modules (one with corner and one without corner) have been designed and fabricated according to the 1 : 3 reduced scale. In addition, quasi-static loading test and finite element value simulation have been performed; the destruction process, destroy mode, bearing capacity, hysteretic behavior, etc., have been studied, and the impact of the axial compression ratio on the bearing capacity of the modular unit has been mainly discussed. Based on the analysis results, the lateral resistance calculation model of the box-plate steel structure modular unit has been put forward, which has provided basis for the establishment of the lateral resistance calculation method.

2. Test Research

2.1. Design of Test Piece. To further reflect the overturning moment at the bottom of the high-rise structure and consider the impact of boundary stiffness on the space modular unit, three-storey single typical space modular unit has been selected as the study object during the test design. Suppose that the interstorey sheer force among the three adjoining storeys is the same, set the loading beam on the upper edge of the upper-storey gable, and set the lower part of model as the fixed end, as shown in Figure 2. Under this simplified way, the middle-storey modular unit is little affected by the boundary stiffness, which can more truly reflect the stress-bearing performance of the box-plate steel structure modular unit. Take scaled design to the prototype structure according to the 1 : 3 reduced scale, and the size of the test piece after measuring is as follows: length: 1,800 mm; width: 1,200 mm; storey height: 1,000 mm; wall thickness: 3 mm; plate thickness: 3 mm. Two test pieces have been designed and fabricated, in which test piece 1 has no corner reinforcing structure measure and test piece 2 has set 120 mm × 120 mm closed stiffeners with a thickness of 5 mm at four corners. The size of the test piece and the size of "T-" and "L-" shaped stiffeners are shown in Table 1.

2.2. Material Properties. The steel plate wall and stiffener shall be Q235 B steel. Through the material property test [22], the mechanical performance parameters of steel under the unilateral stretching state have been determined, and the test results are shown in Table 2.

2.3. Test Unit and Loading System. Anchor beam is welded at the surrounding of the lower storey of the test piece. During the test process, the anchor beam has been connected with reserved ground anchor hole of laboratory through the ground anchor bolt so as to reach the effect of fixing the bottom of the test piece. The upper edge of a unilateral gable of the upper storey of test piece is welded with the loading beam. During the test process, one end of the loading beam

(a) (b)

Figure 1: Application of the box-plate structure system: (a) structural system; (b) design of the multifunctional integrated board.

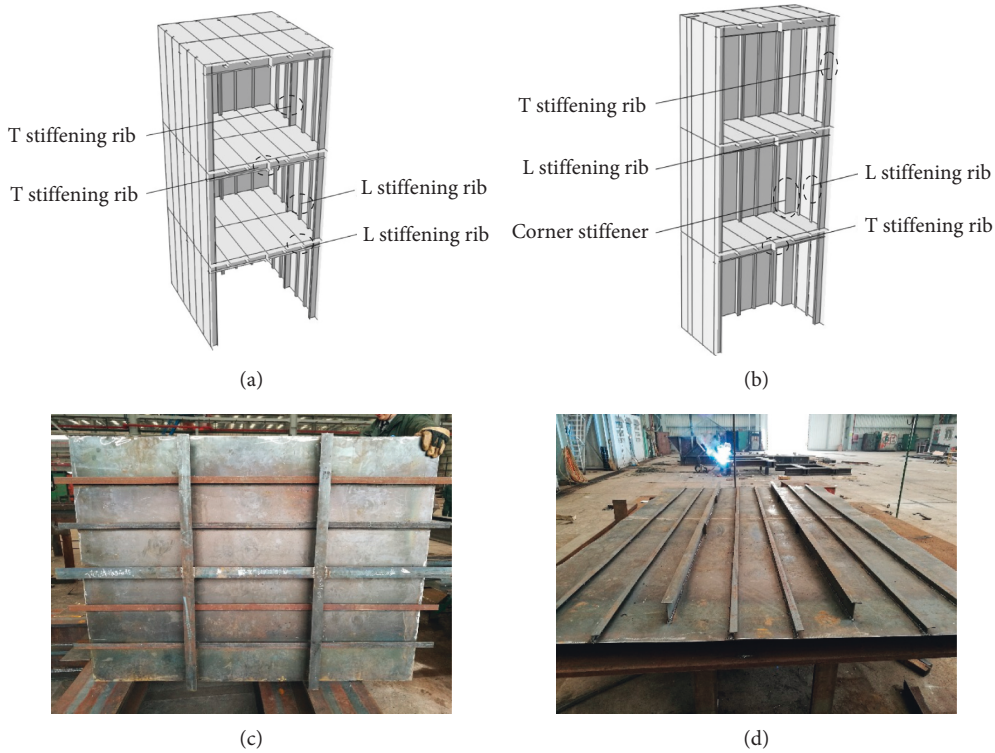

(a) (b)

(c) (d)

Figure 2: Schematic of the unit module: (a) cross section of test model no.1; (b) cross section of test model no. 2; (c) processing production of the floor slab with rib stiffener; (d) processing production of the wallboard with rib stiffener.

Table 1: Size of the stiffening rib.

Position	T stiffening rib (mm)	L stiffening rib (mm)
Wall	T70 × 3/35 × 4	L25 × 25 × 3
Plate	T85 × 4/50 × 5	L30 × 30 × 3

Table 2: Test results of steel properties.

Steel plate thickness	3 mm	4 mm	5 mm
Modulus of elasticity (GPa)	221.959	213.074	199.459
Yield strength (MPa)	331	310	304
Ultimate strength (MPa)	487	465	461
Fracture strain (%)	20.1	22.3	24.4
Strong flexion ratio	1.47	1.50	1.52

is connected with horizontal jack. The vertical jack distributes the vertical load to the loading beam of two sides through the distribution beam. Set 1 displacement meter at each side of unilateral horizontal jack, respectively, to monitor the loading process. Set 3 displacement meters at the elevation places of the second- and third-storey floor and set 1 displacement meter at the corresponding position of a bilateral gable anchor beam to monitor the support displacement. The test unit and displacement monitoring points are shown in Figure 3.

During the test process, the vertical load is obtained through the conversion of $F/(Af_y) = 0.1$, in which F is the total vertical load, A is the sum of sectional area of a

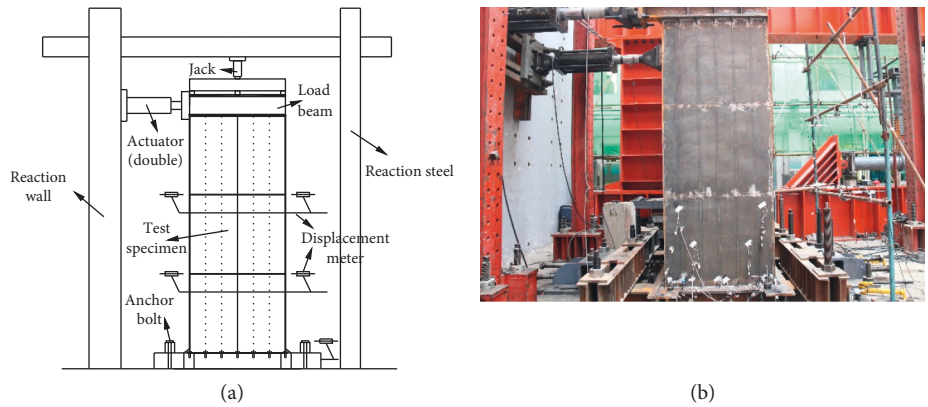

Figure 3: Test equipment and displacement measuring point layout: (a) sketch map; (b) actual loading diagram.

unilateral gable and stiffener, and f_y is the material's yield stress. Keep the vertical load unchanged and inflict horizontal thrust and then synchronously take equivalent load to the bilateral horizontal jack. In accordance with the provision of *Seismic Test Procedures of Building* [23], the loading mode shall adopt variable amplitude displacement to control the load. Circulate twice for each level of displacement and take 2 mm for displacement increment before yield and 0.5δ after yield, in which δ is the yield displacement, and the horizontal load system is shown in Figure 4.

2.4. Destruction Process and Destroy Mode of Test Piece

2.4.1. Destruction Process and Destroy Mode of Test Piece 1. At the initial stage of loading, test piece 1 is at the elastic stage and the loading displacement is little without obvious phenomenon. When the bilateral horizontal actuators are loaded to 8 mm of horizontal displacement synchronously, the strain of the strain gauge at the four corners of gable at the bottom of the test piece has exceeded 1491 $\mu\varepsilon$. According to the material property test result, the four corners of gable positions at the bottom of the test piece have been yielded. Continue loading to 12 mm of horizontal displacement; the loading-displacement hysteresis curve of bilateral loading points is open slightly, and the test piece has been yielded at this time. When loading to 24 mm of horizontal displacement, the corner of the test piece has large buckle and deformation for the first time, as shown in Figure 5(a); when loading to 28 mm of horizontal displacement, the four corners of the bottom of the test piece have large buckling and deformation, and the deformation cannot be recovered with the reverse unloading. At that time, the test piece reaches the limit value of horizontal thrust, which is about 650 kN. Then, the horizontal force-load beam end displacement curve proceeds to the descending stage. When the bilateral horizontal actuator is loaded to 36 mm of horizontal displacement, the four corners of the bottom of test piece start tearing, as shown in Figure 5(b); when the horizontal displacement is continued to be loaded up to 44 mm, the four corners of the bottom of test piece are torn obviously and the horizontal bearing force has been descended to 85% of limit bearing force. At that time, loading shall be stopped.

During the whole loading process, since the corner stiffness of test piece 1 is little, the gable is not yielded by shearing and the wallboard shear behavior is not made full use, and the plastic deformation mainly occurs at the bottom of the whole test piece, presenting bending failure form, as shown in Figure 5(c). At the late stage of loading for the test piece, the wallboard vertical to the loading direction has corresponding destruction due to the fracture of welded stiffeners. The bottom of the test piece is destroyed under overturning moment. The ultimate bearing capacity of the test piece descends quickly, and the ductility and energy dispassion are poor.

2.4.2. Destruction Process and Destroy Mode of Test Piece 2. At the initial stage of loading, test piece 2 is at the elastic stage and the loading displacement is little without obvious phenomenon. When the bilateral horizontal actuators are loaded to 8 mm of horizontal displacement synchronously, the strain of strain gauge at the four corners of gable at the bottom of the test piece exceeds 1491 $\mu\varepsilon$. According to the material property test result, the four corners of gable steel plates at the bottom of the test piece have been yielded. Continue loading to 12 mm of horizontal displacement; it can be seen that the bottom gable of the test piece is generally yielded through bottom strain gauge monitoring data, and the loading-displacement curve slope of bilateral loading points start changing. When the horizontal displacement is loaded to 24 mm, the four corners of the bottom of the test piece have deformation, as shown in Figure 6(a). When the horizontal displacement is loaded to 36 mm, the corners of the bottom of the test piece firstly appear tear, as shown in Figure 6(b). At that time, the test piece reaches the limit value of horizontal thrust, which is about 920 kN. Then, the bilateral horizontal thrust-loading beam end displacement curve proceeds to the descending stage. When the horizontal displacement of test piece 2 is loaded to 54 mm, the four corners of the bottom of the test piece have serious deformation, as shown in Figure 6(c). At that time, the bearing capacity descends to 85% of ultimate bearing capacity and loading shall be stopped.

When the reinforcing structure at the bottom of test piece 2 appears tear after gable wallboard is yielded, the test

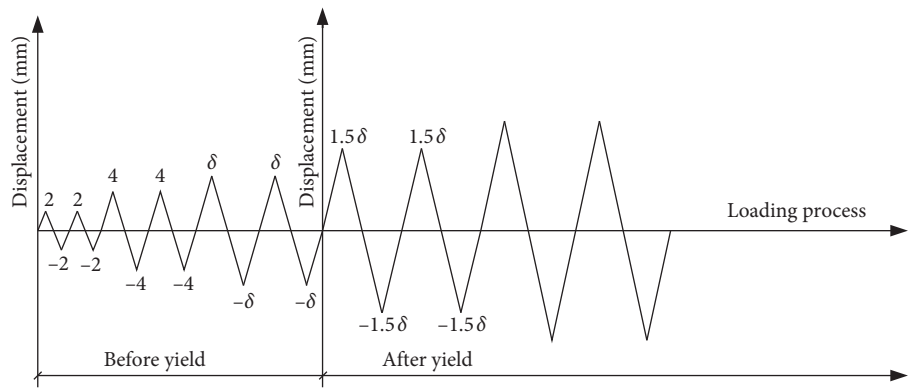

Figure 4: Loading system.

(a) (b) (c)

Figure 5: Failure process of specimen 1: (a) buckling of bottom corner; (b) tear of bottom corner; (c) ultimate destruction.

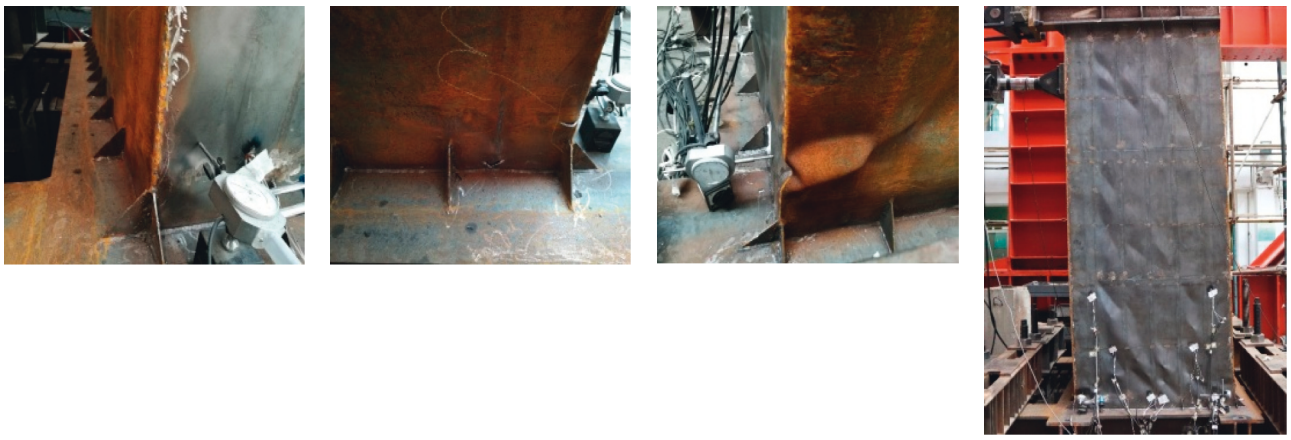

(a) (b) (c) (d)

Figure 6: Failure process of specimen 2: (a) deformation in the bottom; (b) corner stiffener tear; (c) the corners are badly deformed; (d) ultimate destruction.

piece has reached the limit bearing force. Compared with the plastic deformation of test piece 1, which is mainly concentrated at the root of gable, the plastic deformation of gable of test piece 2 is uniform, as shown in Figure 6(d). The destruction form of test piece 2 is shear destruction; the shearing performance of gable wallboard has been made full use, so it has higher bearing capacity and larger deformability.

2.5. Test Results Analysis

2.5.1. Hysteresis Curve and Skeleton Curve. The characteristic load, characteristic displacement, and ductility coefficient of all test pieces are shown in Table 3.

It can be seen from Table 3 that the ductility coefficients of two tested models are more than 2 and less than 3 because the thickness of the wall plate is thin [24]. And in comparison, the characteristic load and characteristic displacement and ductility of test piece 2 are larger than that of test piece 1, which means that corner reinforcing structure measures can improve the ductility of the test piece to certain degree while enhancing the bearing capacity.

To study the force bearing performance of the space modular unit under boundary constraint, we take the middle storey as object; the hysteresis curve is shown in Figure 7, and the skeleton curve is shown in Figure 8. Through the comparison of the hysteresis curve and skeleton curve, the following points are noted: (1) the interstorey shear-displacement hysteresis curve of test piece 1 and test piece 2 basically presents linear relation with large slope at the initial stage. The hysteresis curve contains little area, and the test piece is at the elastic working stage, with large initial lateral stiffness; with the continuous increase of loading displacement, the test piece will start yielding, and the interstorey shear displacement will present obvious nonlinearity. The curve slope will be smaller, and the hysteresis curve will be opened gradually. The area that every hysteresis loop contains will be increased, and the test piece will start entering the overall yield working stage. (2) The hysteresis curve of test piece 2 is more plump than that of test piece 1, and the reason is that test piece 1 will have bottom buckling and destruction under the bottom overturning moment effect and the plastic deformation is mainly concentrated on the bottom storey; however, test piece 2 can enable the gable wallboard to give full play to shear performance under the corner reinforcing structure effect. (3) The skeleton curve of test piece 1 and test piece 2 has elastic stages, elastic-plastic stage, and decline stage. Due to the existence of the corner reinforcing structure, test piece 2's stiffness and ultimate bearing capacity as well as yield displacement at elastic stage are larger than that of test piece 1 and the bearing capacity descends slowly.

2.5.2. Ductility and Energy Dissipation. The ductility coefficient μ of displacement is the ratio between limit interstorey displacement Δ_u and yield interstorey displacement Δ_y. The Δ_u shall be the corresponding interstorey displacement when the load descends to $0.85P_m$ (P_m is the limit load), and Δ_y shall be determined by the energy equivalent method; the variation curve of the equivalent viscous damping ratio of all test pieces with interstorey displacement angle is shown in Figure 9.

Figure 9 shows that the growing speed of equivalent viscous damping ratio of test piece 2 with the variation of interstorey displacement angle is larger than that of test piece 1. Before the interstorey displacement angle is about 0.9%, the equivalent viscous damping ratio of test piece 1 is larger than that of test piece 2; with the increase of interstorey displacement angle, the equivalent viscous damping ratio of test piece 2 gradually exceeds that of test piece 1. The reason behind it is that the corner reinforcing structure measures have made the equivalent viscous damping ratio of test piece 2 larger at the late stage of yield and improved the energy dissipation of test piece, while for test piece 1, the steel plate wall exited the work early at the late stage of yield. It therefore has further proved the aforesaid conclusion: corner reinforcing structure measures can make the test piece make full use of the shear behavior of wallboard.

2.5.3. Stiffness Degradation. According to the provisions of GB50011-2010 *Code for Seismic Design of Buildings* [25], loop stiffness is adopted to represent the stiffness degradation of test piece, as shown in Figure 10. It can be seen from Figure 10 that the stiffness of test piece 2 is larger than that of test piece 1; the stiffness of two test pieces is degraded; due to the existence of corner reinforcing structure measures, the stiffness of test piece 2 is degraded slowly at the early stage; the stiffness of two test pieces at the late loading stage is uniform and stable.

3. Numerical Simulation

3.1. Model Hypothesis. ABAQUS [26] is selected in this paper to take finite element modeling and analysis to the two box-plate steel structure modular unit test pieces in the test. In the finite element model, the unit type is S4R (four-node linear decrement integral shell unit); to guarantee the convergence of calculation results, after cutting the ribbed shell unit, use quadrilateral-dominated structure classification method to take meshing to the model; considering the initial geometry defect of the test piece during the actual test, before model calculation is submitted, introduce the first 3-order buckling model of the calculation model under the bilateral horizontal thrust effect as the initial geometry defect distribution and take the amplitude $\lambda/500$, in which λ is the single-layer gable height-thickness ratio. The steel structure shall be ideal elastic plasticity. According to the material characteristic test result, the steel elastic modulus is 2.21×10^5 MPa and the yield strength is 331 MPa. The material characteristics are shown in Table 2.

3.2. Comparative Analysis of Finite Element Results and Test Results. The comparison between the finite element analysis results and test destruction form of two test pieces is shown in Figure 11. The comparison of the hysteresis curve and skeleton curve is, respectively, shown in Figures 12 and 13.

Table 3: Characteristic displacement and load of the specimens.

Number	Direction	P_y (kN)	Δ_y (mm)	P_m (kN)	Δ_m (mm)	P_u (kN)	Δ_u (mm)	μ
No. 1	Positive	607.99	3.8	652.27	5.1	554.43	7.7	2.03
	Negative	−553.11	−3.8	−604.74	−5.8	−514.13	−7.8	2.05
No. 2	Positive	771.65	4	917.79	6	780.12	9.1	2.28
	Negative	−773.98	−4	−893.97	−6	−759.87	−10.1	2.53

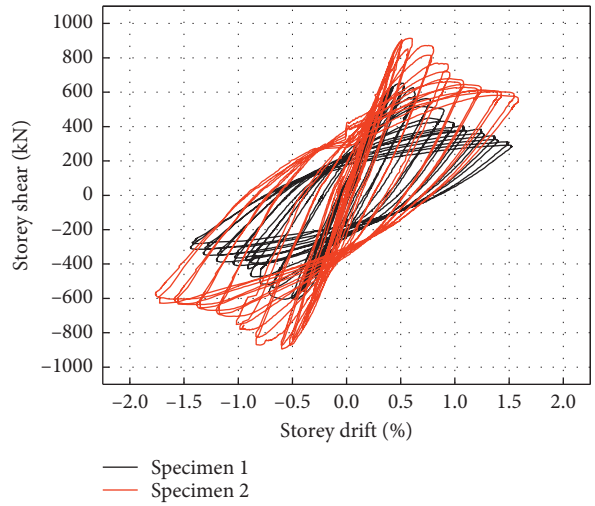

Figure 7: Storey shear versus drift of each specimen.

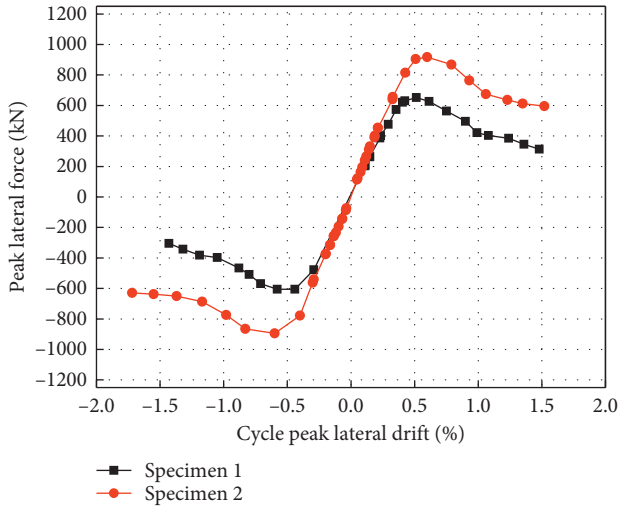

Figure 8: Peak strength envelope.

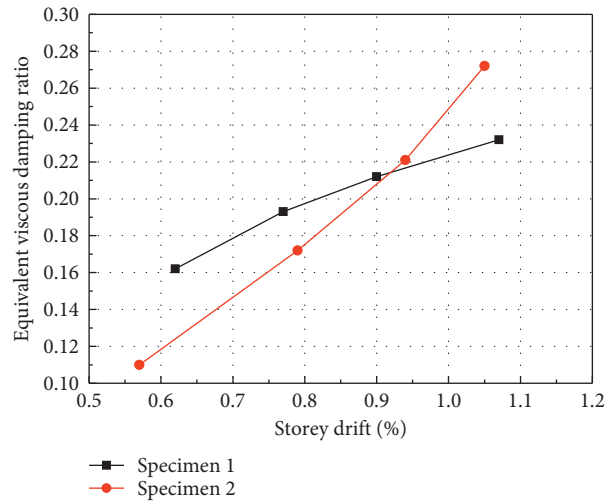

Figure 9: Equivalent viscous damping ratio.

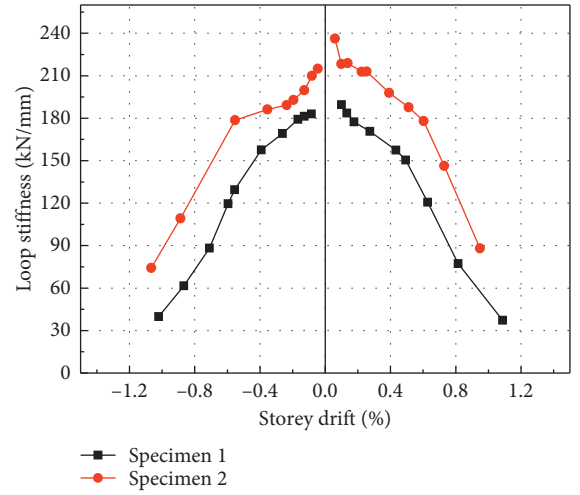

Figure 10: Stiffness degradation trend.

It can be seen from Figure 11 that the destruction mode of finite element numerical simulation of two test pieces is the same as the destruction mode in the specific test: test piece 1 represents the bottom buckling destruction under overturning moment, and the plastic deformation is concentrated at the bottom of the test piece; for test piece 2, it represents the shear destruction of the whole gable, and the plastic deformation is covered on the whole gable. Figures 12 and 13 show that the hysteresis curve and skeleton curve obtained through the finite element model match well with corresponding test results. Therefore, it is reasonable to establish the finite element model in the paper, which can effectively reflect the force bearing performance of the test piece in the test study and can simulate the seismic performance of box-plate steel structure modular unit's seismic performance under low cycle reciprocating load effect.

3.3. Analysis of Influence Parameter. Since box-plate steel structure modular unit vertical multirib wallboard bears the vertical and horizontal effect simultaneously, the impact of

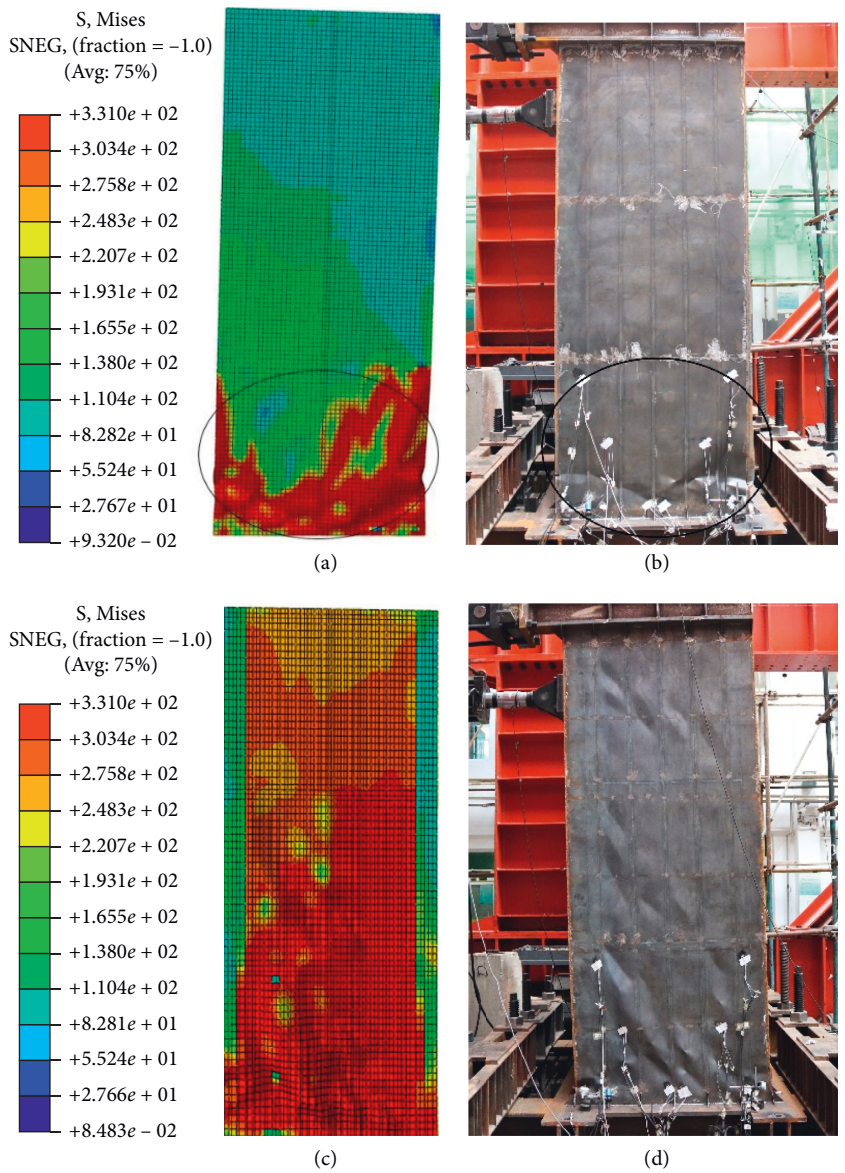

Figure 11: Ultimate destruction: (a) numerical simulation on specimen 1; (b) experimental research on specimen 1; (c) numerical simulation on specimen 2; (d) experimental research on specimen 2.

vertical effect on the modular unit's bearing property can be observed through changing the axial compression ratio n. It has been stipulated in JGJ99-2015 *Technical Regulations for High-rise Civil Building Steel Structure* [27] that the seismic capacity checking column axial compression ratio of steel frame column shall not exceed 0.4. The vertical load of the box-plate steel structure modular unit shall all be borne by wallboard and ribbed stiffeners. It has a larger frame column bearing area compared with other steel plates, so the axial compression ratio n shall be respectively 0.01, 0.05, 0.1, 0.15; β is the flexibility coefficient of corner reinforcing structure rib of the box-plate steel structure modular unit. Specific to the same wallboard height-thickness ratio, β shall be, respectively, 0.7, 0.9, 1.1, and 1.3; λ is the height-thickness ratio of wallboard, and the value is, respectively, 300, 350, 400, and 450; 64 models from four groups are taken for finite element analysis, and the statistical parameters are shown in Table 4. The analysis result of each group is shown in Figures 14–16.

3.3.1. Influence of λ on Bearing Capacity of Model. From Figure 14, it can be seen that the ultimate bearing capacity of the model varies with the height-thickness ratio of the wallboard under different axial loads. With the increase of the height-thickness ratio of the wallboard, the ultimate bearing capacity of the model decreases, and the ultimate bearing capacity of the model decreases from about 1500 kN to about 1000 kN in the range of the height-thickness ratio of the wallboard from 300 to 450. The multiribbed wallboard of the spatial stress element usually does not buckle before yielding under shear force. The shear bearing capacity of the wallboard is the product of the area of the section of the

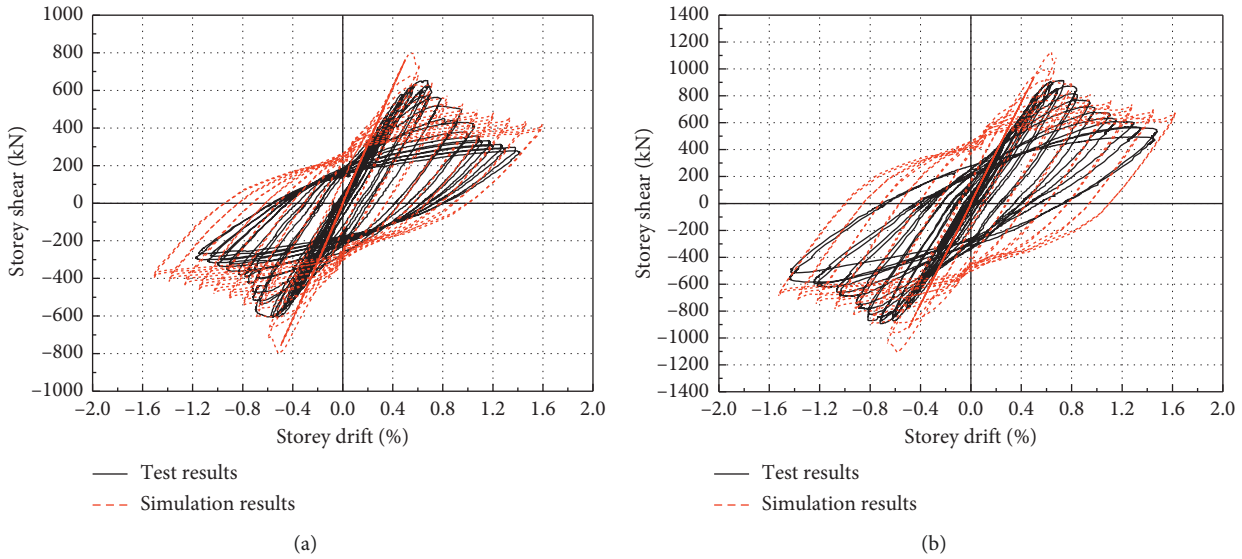

Figure 12: Storey shear versus drift of numerical simulation and experimental study: (a) specimen 1; (b) specimen 2.

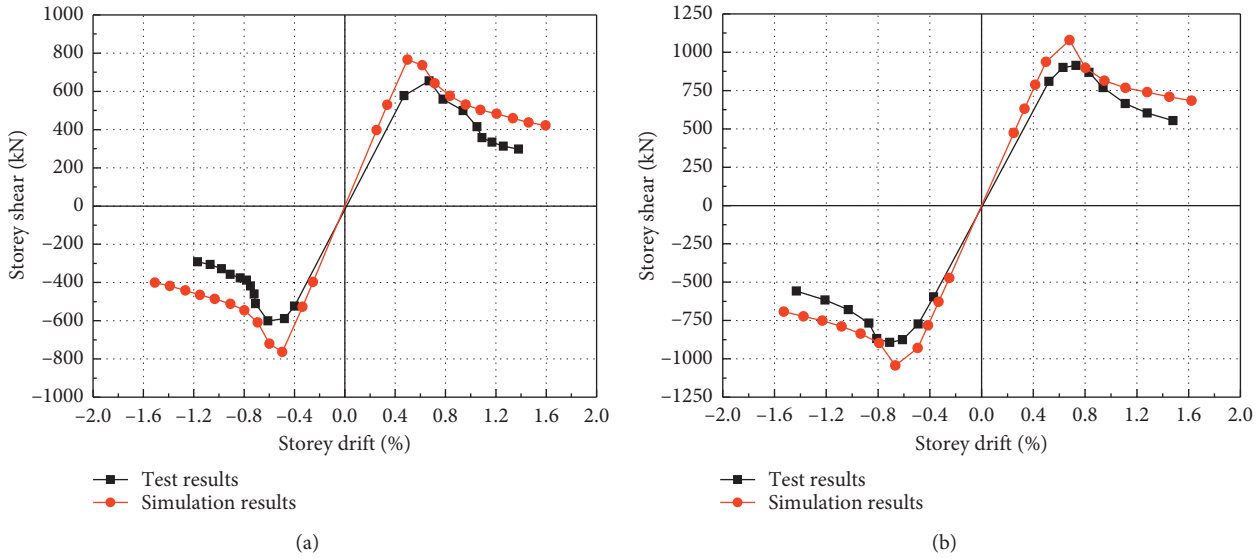

Figure 13: Peak strength envelope of numerical simulation and experimental study: (a) specimen 1; (b) specimen 2.

wallboard subjected to shear and the shear yield stress of the wallboard material. Therefore, the ratio of height to thickness of the wallboard is the most direct factor affecting the shear bearing capacity of the wallboard under certain material conditions. After the reinforcement measures are set at the corner of the model, the compressive failure under the overturning moment at the bottom of the model is changed into the shear yield failure of the gable wall panels. Therefore, it has more obvious influence on the ultimate bearing capacity of the model after the reinforcement measures are set at the corner of the model. It shows that the ultimate bearing capacity decreases with the increase of the height-thickness ratio of the wallboard.

3.3.2. Influence of β on Bearing Capacity of Model. From Figure 15, it can be seen that the ultimate bearing capacity increases with the increase of the structural flexibility adjustment coefficient at the corner of the model. Compared with the trend of the ultimate bearing capacity changing with the height-thickness ratio of the wallboard, the trend of the model ultimate bearing capacity changing with the structural flexibility adjustment coefficient at the corner of the model is smaller because the stiffness of the model corner reinforcement rib is changed by the increase of the structural flexibility coefficient and the section of the model corner reinforcement rib. For example, when the ratio of height to thickness is 300, the adjustment coefficient of structural

Table 4: Main parameters of the finite element model.

Serial number	λ	Wall thickness (mm)	β	Moment of inertia of angular reinforcement (mm^4)	Corner rib (mm × mm × mm)	n
1	300	3.33	0.7	6626081	120 × 120 × 5.7	0.01
2	300	3.33	0.7	6626081	120 × 120 × 5.7	0.05
3	300	3.33	0.7	6626081	120 × 120 × 5.7	0.10
4	300	3.33	0.7	6626081	120 × 120 × 5.7	0.15
5	300	3.33	0.9	8519247	120 × 120 × 7.4	0.01
6	300	3.33	0.9	8519247	120 × 120 × 7.4	0.05
7	300	3.33	0.9	8519247	120 × 120 × 7.4	0.10
8	300	3.33	0.9	8519247	120 × 120 × 7.4	0.15
9	300	3.33	1.1	10412414	120 × 120 × 9.0	0.01
10	300	3.33	1.1	10412414	120 × 120 × 9.0	0.05
11	300	3.33	1.1	10412414	120 × 120 × 9.0	0.10
12	300	3.33	1.1	10412414	120 × 120 × 9.0	0.15
13	300	3.33	1.3	12305580	120 × 120 × 10.6	0.01
14	300	3.33	1.3	12305580	120 × 120 × 10.6	0.05
15	300	3.33	1.3	12305580	120 × 120 × 10.6	0.10
16	300	3.33	1.3	12305580	120 × 120 × 10.6	0.15
17	350	2.86	0.7	5690869	120 × 120 × 4.9	0.01
18	350	2.86	0.7	5690869	120 × 120 × 4.9	0.05
19	350	2.86	0.7	5690869	120 × 120 × 4.9	0.10
20	350	2.86	0.7	5690869	120 × 120 × 4.9	0.15
21	350	2.86	0.9	7316831	120 × 120 × 6.3	0.01
22	350	2.86	0.9	7316831	120 × 120 × 6.3	0.05
23	350	2.86	0.9	7316831	120 × 120 × 6.3	0.10
24	350	2.86	0.9	7316831	120 × 120 × 6.3	0.15
25	350	2.86	1.1	8942794	120 × 120 × 7.8	0.01
26	350	2.86	1.1	8942794	120 × 120 × 7.8	0.05
27	350	2.86	1.1	8942794	120 × 120 × 7.8	0.10
28	350	2.86	1.1	8942794	120 × 120 × 7.8	0.15
29	350	2.86	1.3	10568756	120 × 120 × 9.2	0.01
30	350	2.86	1.3	10568756	120 × 120 × 9.2	0.05
31	350	2.86	1.3	10568756	120 × 120 × 9.2	0.10
32	350	2.86	1.3	10568756	120 × 120 × 9.2	0.15
33	400	2.5	0.7	4974536	120 × 120 × 4.3	0.01
34	400	2.5	0.7	4974536	120 × 120 × 4.3	0.05
35	400	2.5	0.7	4974536	120 × 120 × 4.3	0.10
36	400	2.5	0.7	4974536	120 × 120 × 4.3	0.15
37	400	2.5	0.9	6395832	120 × 120 × 5.5	0.01
38	400	2.5	0.9	6395832	120 × 120 × 5.5	0.05
39	400	2.5	0.9	6395832	120 × 120 × 5.5	0.10
40	400	2.5	0.9	6395832	120 × 120 × 5.5	0.15
41	400	2.5	1.1	7817128	120 × 120 × 6.8	0.01
42	400	2.5	1.1	7817128	120 × 120 × 6.8	0.05
43	400	2.5	1.1	7817128	120 × 120 × 6.8	0.10
44	400	2.5	1.1	7817128	120 × 120 × 6.8	0.15
45	400	2.5	1.3	9238424	120 × 120 × 8.0	0.01
46	400	2.5	1.3	9238424	120 × 120 × 8.0	0.05
47	400	2.5	1.3	9238424	120 × 120 × 8.0	0.10
48	400	2.5	1.3	9238424	120 × 120 × 8.0	0.15
49	450	2.22	0.7	4417387	120 × 120 × 3.8	0.01
50	450	2.22	0.7	4417387	120 × 120 × 3.8	0.05
51	450	2.22	0.7	4417387	120 × 120 × 3.8	0.10
52	450	2.22	0.7	4417387	120 × 120 × 3.8	0.15
53	450	2.22	0.9	5679498	120 × 120 × 4.9	0.01
54	450	2.22	0.9	5679498	120 × 120 × 4.9	0.05
55	450	2.22	0.9	5679498	120 × 120 × 4.9	0.10
56	450	2.22	0.9	5679498	120 × 120 × 4.9	0.15
57	450	2.22	1.1	6941609	120 × 120 × 6.0	0.01
58	450	2.22	1.1	6941609	120 × 120 × 6.0	0.05
59	450	2.22	1.1	6941609	120 × 120 × 6.0	0.10
60	450	2.22	1.1	6941609	120 × 120 × 6.0	0.15

Table 4: Continued.

Serial number	λ	Wall thickness (mm)	β	Moment of inertia of angular reinforcement (mm^4)	Corner rib (mm × mm × mm)	n
61	450	2.22	1.3	8203720	120 × 120 × 7.1	0.01
62	450	2.22	1.3	8203720	120 × 120 × 7.1	0.05
63	450	2.22	1.3	8203720	120 × 120 × 7.1	0.10
64	450	2.22	1.3	8203720	120 × 120 × 7.1	0.15

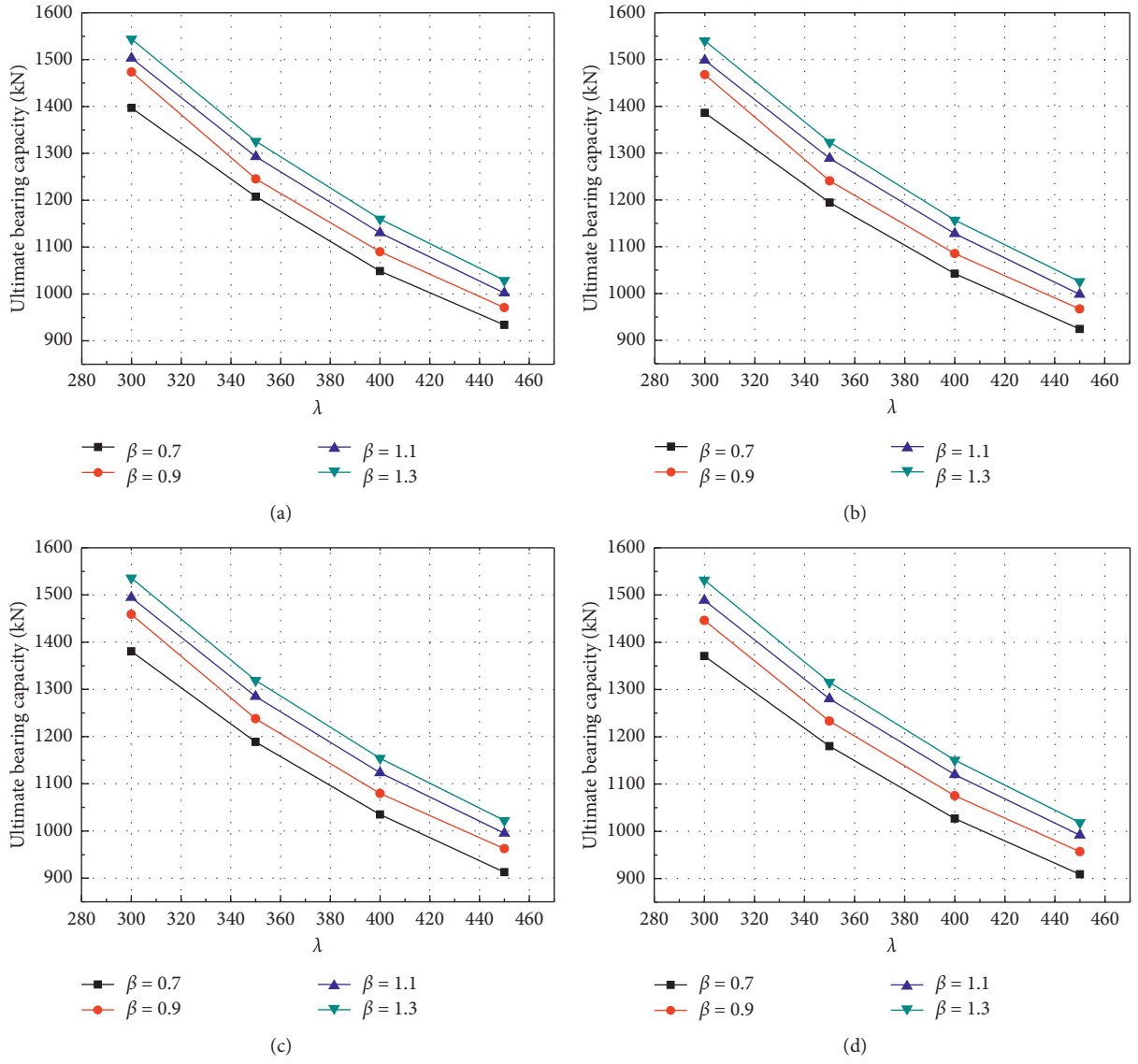

Figure 14: Influence of λ on ultimate bearing capacity of model: (a) $n = 0.01$; (b) $n = 0.05$; (c) $n = 0.1$; (d) $n = 0.15$.

flexibility at the corner of the model changes from 0.7 to 1.3, and the ultimate bearing capacity of each model generally increases by about 150 kN. In different aspect ratios, the shear yielding capacity of the thin plate is smaller than that of the thick plate, and the strength requirement of the diagonal structure is smaller when the wall plate is fully shear yielding. Therefore, when aspect ratio is 450, the increase of ultimate bearing capacity of the model caused by the change of the structural flexibility coefficient from 0.7 to 1.3 is smaller than that of the model with height-thickness ratio of 300 under the same condition.

3.3.3. Influence of n on Bearing Capacity of Model. From Figure 16, it can be seen that the ultimate bearing capacity of all the models decreases with the increase of the model axial compression ratio when the wallboard height-thickness ratio λ and corner reinforcing structure flexibility coefficient β are

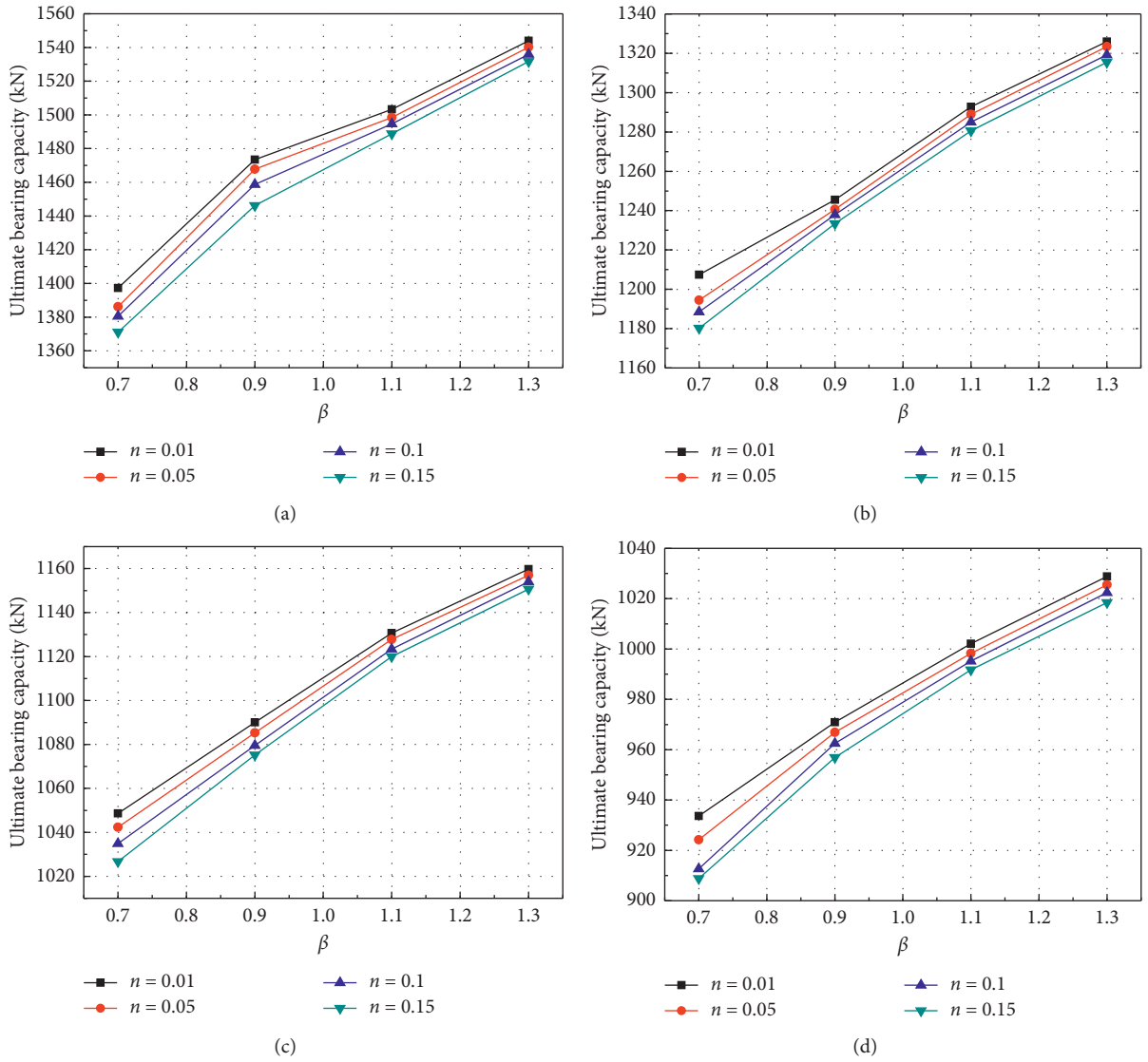

Figure 15: Influence of λ on ultimate bearing capacity of model: (a) $\lambda = 300$; (b) $\lambda = 350$; (c) $\lambda = 400$; (d) $\lambda = 450$.

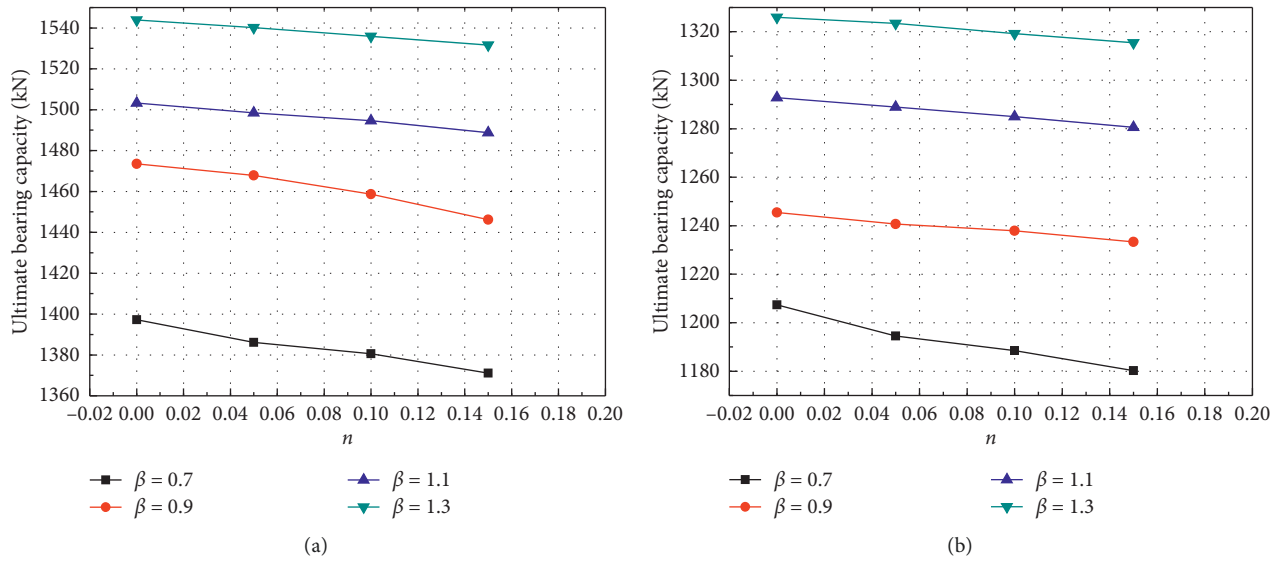

Figure 16: Continued.

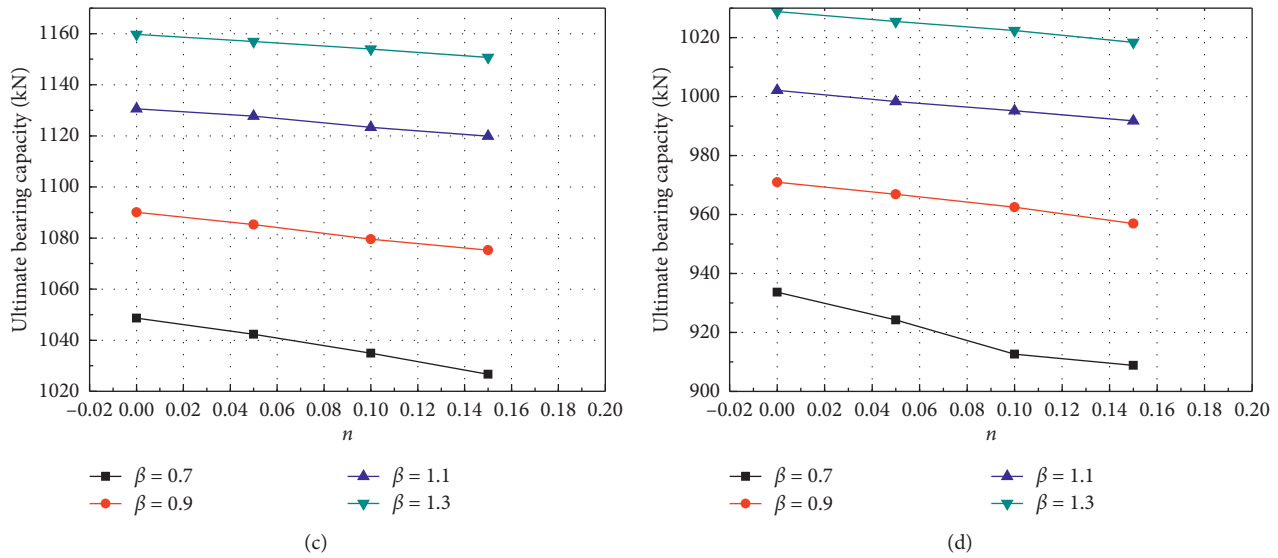

Figure 16: Analysis result diagram of each group: (a) $\lambda = 300$; (b) $\lambda = 350$; (c) $\lambda = 400$; (d) $\lambda = 450$.

certain. But the influence degree is little because the existence of the axial compression ratio has reduced the ultimate bending moment of the corner reinforcing structure rib under a horizontal effect and further reduced the bearing capacity of single cross-frame constituted by reinforcing structure rib and loading beam.

4. Lateral Load Resistance Calculation Model

Based on the above destruction model and parameter analysis result, what plays an important role in the bearing capacity of the test piece is the model bottom bearing. Axial compression ratio has little influence on the bearing capacity of model, so the influence will not be considered, and lateral load resistance calculation model has been put forward to the modular unit with or without the corner reinforcing structure rib.

4.1. Modular Unit without Corner Reinforcing Structure. When the box-plate steel structure module-bearing unit has no structure measures, the bottom storey will be yielded when the test piece is destroyed, but the wallboard is not yielded by shearing, and the shearing behavior will not be given full play to. The destruction mode is the structure bottom steel plate's buckling caused by overturning moment. When calculating the bearing capacity, the calculation model could be the bottom section of model, and the ultimate bearing capacity of modular unit can be calculated according to the bottom section ultimate bending moment. When calculating the bottom section limit bending moment, it can be simplified by taking half of section according to the symmetry of the model section and the final ultimate bending moment shall be the sum of two symmetrical section ultimate bending moments. The lateral resistance calculation model is shown in Figure 17, in which the wallboard stiffener is equivalent to wallboard section thickness according to the principle of equivalent. The ultimate stress of the section compression zone shall be the stable-controlled stress before section equivalent and the lateral bearing capacity can be calculated according to the following formula:

$$V = \frac{2M}{H}, \tag{1}$$

where M is the ultimate moment of half section and H is the height.

4.2. Modular Unit with Corner Reinforcing Structure. According to the test and finite analysis result, the corner structure measures can avoid the space bearing unit from bending destruction so that the modular unit will make full use of the shearing behavior of wallboard. The corner reinforcing structure of the box-plate steel structure space-bearing unit has certain stiffness, and the bilateral reinforcing structure and top beam of gable are similar with a single cross frame. When the test piece is destroyed, the bilateral gable wallboard shall be yielded by shearing force, and the reinforcing structure bottom of the test piece will reach ultimate bending moment and the destruction mode is the corner destruction caused by the horizontal shear. When calculating the lateral bearing capacity, the calculation model can be simplified into units composed of bilateral gable and middle part. As shown in Figure 18, the lateral bearing force is composed of bilateral gable part and middle part.

Ignoring the flexural stiffness of the floor in the plane of the gable wall, the approximate formula (2) is used to calculate the ultimate lateral bearing capacity of the frame when the reinforced part at the bottom of the model reaches the ultimate bending moment of the section:

$$V_f = \frac{(4M_c - 2N\delta)}{H}, \tag{2}$$

where M_c is the ultimate moment of corner reinforcement under bending and compression, H is the height, N is the

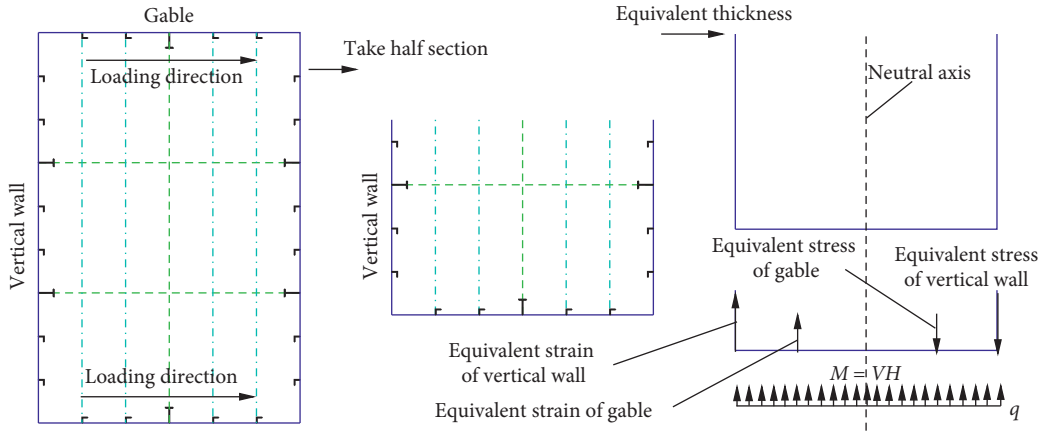

Figure 17: Calculation model of lateral force of the module element without angular reinforcement.

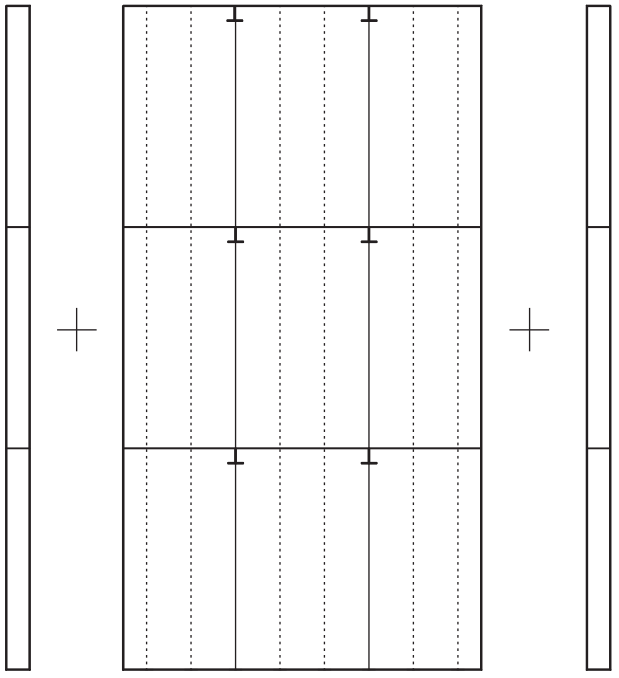

Figure 18: Calculation model of lateral force of the module element with angular reinforcement (gable + middle + gable).

vertical pressure on the top corner of a space stress element, and δ is the lateral displacement of model under ultimate load.

According to the analysis results of the above parameters, the shear bearing capacity of steel wallboard is the shear yield capacity of the whole section, which can be calculated as follows:

$$V_p = \tau_y b t_w = \left(\frac{f_y}{\sqrt{3}}\right) b t_w, \tag{3}$$

where b is the width of the wall shear panels, t_w is the thickness of the wall panels, and f_y is the yield strength of materials.

According to the analysis results of the above parameters, the tension and compression stress of the stiffening rib at the bottom of the space element is small when it reaches the ultimate bearing capacity, so only the action of the wall plate is considered when calculating the bending moment at the bottom of the middle part. The tension and compression stress on the bottom wall of the middle part are $0.3f_y$. The bottom moment of the middle part can be calculated as follows:

$$V_m = 0.3 f_y A_m b_m, \tag{4}$$

where A_m is the area of one-sided wallboard in the middle part, b_m is the spacing between wall panels on both sides of the middle part, and f_y is the yield strength of materials.

The ultimate lateral bearing capacity of three-storey spatial stress element of the box-plate steel structure can be calculated as follows:

$$V = 2\left(V_f + V_p\right) + V_m. \tag{5}$$

5. Conclusions

Through taking test and finite element simulation to three-storey single open box-plate steel structure modular units by setting or not setting corner reinforcing structure, the destruction process, hysteresis curve, skeleton curve, and bearing capacity have been compared and analyzed, the impact of the axial compression ratio on the modular unit has been discussed, and the following conclusions are obtained:

(1) The destruction of two test pieces starts from the cracks at the corner of the bottom. For the space modular unit without corner reinforcing structure measures, the plastic deformation at final destruction mainly occurs at the bottom of the test piece, which is destroyed by buckling, while the bearing capacity is controlled by the bottom overturning moment; for the space modular unit with corner reinforcing structure measures, the bottom gable is generally yielded before destruction and during final destruction, and the upper and lower three-storey gable plastic deformation is uniform, representing shearing destruction form. Compared with test piece

without the corner reinforcing structure, it has made better use of the shearing behavior of gable wallboard.

(2) The corner reinforcing structure measure has enhanced the ultimate bearing capacity of the modular unit test piece and lateral stiffness at the elastic stage in certain degree, which has improved the ductility performance and energy dissipation at the late stage of yield.

(3) The ultimate bearing capacity of the structural unit decreases with the increase of wall thickness ratio λ; the ultimate bearing capacity increases with the increase of structural flexibility coefficient β at the corner of the structural unit; when the wallboard height-thickness ratio λ and corner reinforcing structure flexibility coefficient β are certain, axial compression ratio n has little influence to ultimate bearing capacity.

(4) The calculation model of the modular unit with or without corner reinforcing structure rib has been put forward: the destruction model of the modular unit without the corner reinforcing structure rib is controlled by the bottom overturning moment, and the lateral calculation model is the model bottom section; the destruction model of the modular unit with the corner reinforcing structure rib is corner destruction caused by horizontal shear force, and the gable wallboard is stressed uniformly. Therefore, the calculation model is simplified into units composed of two sides of gable and middle part. And the calculation formula for the ultimate lateral bearing capacity of the three-storey spatial stress element of the box-plate steel structure has been proposed based on results of the test and simulation.

Data Availability

The data used to support the findings of this study are included in the article and available from the corresponding author upon request.

Conflicts of Interest

We confirm that there are no conflicts of interest.

Acknowledgments

The financial support was provided by the Beijing Urban Planning & Land Resources Management Committee (2017-016) and Technological Innovation and Research and Development Foundation of CSIC (201815K).

References

[1] A. Razzazzadeh and F. R. Mashiri, "Analysis of steel plate shear walls," in *Proceedings of the fourth International Conference on Steel and Composite Structures*, Sydney, Australia, July 2010.

[2] M. Elgaaly and Y. Liu, "Analysis of thin-steel-plate shear walls," *Journal of Structural Engineering*, vol. 123, no. 11, pp. 1487–1496, 1997.

[3] J. J. Men, Q. X. Shi, and Z. J. He, "Optimal design of tall residential building with RC shear wall and with rectangular layout," *International Journal of High-Rise Buildings*, vol. 3, no. 4, pp. 285–296, 2014.

[4] D. J. L. Kennedy, G. L. Kulak, and R. Driver, "Discussion of " postbuckling behavior of steel-plate shear walls under cyclic loads" by M. Elgaaly, V. Caccese, and C. Du (February, 1993, vol. 119, no. 2)," *Journal of Structural Engineering*, vol. 120, no. 7, pp. 2250-2251, 1994.

[5] K. C. Tsai and Y. C. Lin, "Seismic performance of steel plate shear wall frames," in *Proceedings of the Fourth International Conference on Advances in Steel Structures*, pp. 1179–1186, Shanghai, China, June 2005.

[6] M. Bruneau, C. M. Uang, and R. Sabelli, *Ductile Design of Steel Structures*, McGraw-Hill Professional, New York, NY, USA, 2nd edition, 2011.

[7] C. M. Uang, M. Bruneau, P. Eng, A. S. Whittaker, and K. C. Tsai, *Seismic Design of Steel Structures, The Seismic Design Handbook*, Springer, Boston, MA, USA, 2001.

[8] J. Men and Q. Shi, "ISCS method for the performance-based seismic design of vertically irregular reinforced concrete frame structures," *The Structural Design of Tall and Special Buildings*, vol. 22, no. 11, pp. 887–902, 2013.

[9] M. Elgaaly, "Experimental study on thin steel-plate shear walls under cyclic load," *Journal of Structural Engineering*, vol. 119, no. 2, pp. 573–587, 1993.

[10] R. G. Driver, G. L. Kulak, D. J. L. Kennedy, and A. E. Elwi, "Cyclic test of four-story steel plate shear wall," *Journal of Structural Engineering*, vol. 124, no. 2, pp. 112–120, 1998.

[11] R. G. Driver, G. L. Kulak, A. E. Elwi, and D. J. L. Kennedy, "FE and simplified models of steel plate shear wall," *Journal of Structural Engineering*, vol. 124, no. 2, pp. 121–130, 1998.

[12] E. Kosari, M. Poursha, and K. Abedi, "Seismic evaluation of tall unstiffened steel plate shear wall (SPSW) systems with emphasis on reversal phenomenon in the higher mode pushover curve," *International Journal of Civil Engineering*, vol. 17, no. 5, pp. 523–540, 2018.

[13] N. H. Nguyen and A. S. Whittaker, "Numerical modelling of steel-plate concrete composite shear walls," *Engineering Structures*, vol. 150, pp. 1–11, 2017.

[14] M. Elmatzoglou and A. Avdelas, "08.48: double-steel plate composite shear walls: in-plane seismic behavior," *Ce/papers*, vol. 1, no. 2-3, pp. 2227–2236, 2017.

[15] D. J. Borello, *Behavior and large-scale experimental testing of steel plate shear walls with coupling*, Ph.D. thesis, University of Illinois at Urbana-Champaign, Champaign, IL, USA, 2014.

[16] M. Dastfan and R. Driver, "Large-scale test of a modular steel plate shear wall with partially encased composite columns," *Journal of Structural Engineering*, vol. 142, no. 2, 2016.

[17] W. Wang, L. X. Zhang, S. Q. Su, J. Y. Gao, Y. C. Li, and Y. G. Li, "Experimental research on seismic behavior of corrugated steel plate shear wall," *Journal of Building Structures*, vol. 39, no. 10, pp. 75–84, 2018, in Chinese.

[18] W. Wei, D. X. Long, Z. Y. Feng, C. G. Ling, and C. Y. Yi, "Full-scale cyclic testing of self-centering modular panels for seismic resilient structures," *Key Engineering Materials*, vol. 763, pp. 339–346, 2018.

[19] Y. Ozcelik and P. M. Clayton, "Behavior of columns of steel plate shear walls with beam-connected web plates," *Engineering Structures*, vol. 172, pp. 820–832, 2018.

[20] T. Lan, T. T. Zhao, G. Liu et al., "Finite element analysis of single composite wall in the bottom reinforced zone of box-type steel structure residence," *Steel Structure*, vol. 32, pp. 84–90, 2017, in Chinese.
[21] F. Wu, *Ship Structural Mechanics*, National Defense Industry Press, Beijing, China, 2016, in Chinese.
[22] GB/T 228.1, *Tensile Test of Metallic Materials*, China Planning Press, Beijing, China, 2010, in Chinese.
[23] JGJ 101-2015, *Seismic Test Procedures of Building*, China Architecture & Building Press, Beijing, China, 2015, in Chinese.
[24] T. M. Roberts, "Seismic resistance of steel plate shear walls," *Engineering Structures*, vol. 17, no. 5, pp. 344–351, 1995.
[25] GB50011-2016, *Code for Seismic Design of Buildings*, China Architecture & Building Press, Beijing, China, 2015, in Chinese.
[26] D. Hibbitt, *ABAQUS/Explicit User's Manual*, Hibbitt, Karlsson and Sorensen Inc, Pawtucket, RI, USA, 2010.
[27] JGJ99-2015, *Technical Specification for Steel Structures of High-rise Civil Buildings*, China Architecture & Building Press, Beijing, China, 2016, in Chinese.